OFFICE OF NAVAL RESEARCH

Contract N00014-87-K-0494

R&T Code 400X027YIP

Technical Report No. 8

In-Situ Topographical Imaging of Electrode Surfaces Using High Resolution Phase-Measurement Interferometric Microscopy

by

Henry S. White, David J. Earl, John D. Norton, Harlan J. Kragt

Prepared for Publication in the

Analytical Chemistry

University of Minnesota
Department of Chemical Engineering and Materials Science
Minneapolis, MN 55455

April 10, 1990

SECURITY CLASSIFICATION OF THIS PAGE

REPORT DOCUMENTATION PAGE

1a. REPORT SECURITY CLASSIFICATION Unclassified	1b. RESTRICTIVE MARKINGS
2a. SECURITY CLASSIFICATION AUTHORITY	3. DISTRIBUTION/AVAILABILITY OF REPORT Unclassified/Unlimited
2b. DECLASSIFICATION/DOWNGRADING SCHEDULE	
4. PERFORMING ORGANIZATION REPORT NUMBER(S) ONR Technical Report 8	5. MONITORING ORGANIZATION REPORT NUMBER(S)
6a. NAME OF PERFORMING ORGANIZATION Dept of Chemical Engineering and Materials Science 6b. OFFICE SYMBOL (If applicable) Code 1113	7a. NAME OF MONITORING ORGANIZATION Office of Naval Research
6c. ADDRESS (City, State, and ZIP Code) University of Minnesota Minneapolis, MN 55455	7b. ADDRESS (City, State, and ZIP Code) 800 North Quincy Street Arlington, VA 22217
8a. NAME OF FUNDING/SPONSORING ORGANIZATION Office of Naval Research 8b. OFFICE SYMBOL (If applicable)	9. PROCUREMENT INSTRUMENT IDENTIFICATION NUMBER Contract No. N00014-87-K-0494
8c. ADDRESS (City, State, and ZIP Code) 800 North Quincy Street Arlington, VA 22217-5000	10. SOURCE OF FUNDING NUMBERS PROGRAM ELEMENT NO. / PROJECT NO. / TASK NO. / WORK UNIT ACCESSION NO

11. TITLE (Include Security Classification)

In-Situ Topographical Imaging of Electrode Surfaces Using High Resolution Phase-Measurement Interferometric Microscopy

12. PERSONAL AUTHOR(S)

Henry S. White, David J. Earl, John D. Norton, Harlan J. Kragt

13a. TYPE OF REPORT	13b. TIME COVERED	14. DATE OF REPORT (Year, Month, Day)	15. PAGE COUNT
Technical	FROM 4/10/89 TO 4/10/90	April 10, 1990	25

16. SUPPLEMENTARY NOTATION

prepared for publication in Analytical Chemistry

17. COSATI CODES			18. SUBJECT TERMS (Continue on reverse if necessary and identify by block number)
FIELD	GROUP	SUB-GROUP	

19. ABSTRACT (Continue on reverse if necessary and identify by block number)

Three-dimensional topographical imaging of electrode surfaces using phase-measurement interferometric microscopy is described. Topographical measurements are based on a rapid, non-destructive optical method that provides ultrahigh vertical resolution (0.6 nm) and moderate horizontal resolution (0.5 μm). In-situ images of electrodes prepared from highly oriented pyrolytic graphite, platinum thin films, and polycrystalline iron are reported. In-situ measurement of the time-dependent growth of corrosion pits on Fe in 0.1 M H_2SO_4 is also demonstrated.

20. DISTRIBUTION/AVAILABILITY OF ABSTRACT	21. ABSTRACT SECURITY CLASSIFICATION
☒ UNCLASSIFIED/UNLIMITED ☐ SAME AS RPT ☐ DTIC USERS	Unclassified
22a. NAME OF RESPONSIBLE INDIVIDUAL Henry S. White	22b. TELEPHONE (Include Area Code) (612) 625-6995 22c. OFFICE SYMBOL

DD FORM 1473, 84 MAR 83 APR edition may be used until exhausted. All other editions are obsolete

SECURITY CLASSIFICATION OF THIS PAGE

In-Situ Topographical Imaging of Electrode Surfaces Using High Resolution Phase-Measurement Interferometric Microscopy.

Henry S. White*, David J. Earl, John D. Norton, and Harlan J. Kragt
Department of Chemical Engineering and Materials Science
University of Minnesota
Minneapolis, MN 55455

Abstract. Three-dimensional topographical imaging of electrode surfaces using phase-measurement interferometric microscopy is described. Topographical measurements are based on a rapid, non-destructive optical method that provides ultrahigh vertical resolution (0.6 nm) and moderate horizontal resolution (0.5 μm). *In-situ* images of electrodes prepared from highly oriented pyrolytic graphite, platinum thin films, and polycrystalline iron are reported. *In-situ* measurement of the time-dependent growth of corrosion pits on Fe in 0.1 M H_2SO_4 is also demonstrated.

* Author to whom correspondence should be addressed.

Brief. Phase-measurement interferometric microscopy is used to obtain three-dimensional topographical images of electrode surfaces immersed in aqueous solutions.

Introduction.

Surface topography often plays a crucial role in the interpretation of fundamental electrochemical measurements and in the fabrication of cells. The mainstay of topographical analyses in electrochemistry has been scanning electron microscopy which, although providing nanoscopic resolution, is limited to *ex-situ* analysis. *In-situ* methods of examining electrode topography and physical structure are highly desirable in order to measure potential and time dependent structures that might otherwise be altered by exposing the electrode to air or ultra-high vacuum. Several *in-situ* methods that provide topographical information, either directly or indirectly, are employed to a limited extent in electrochemistry. These include the recent introduction of scanning tunneling microscopy (STM)[1,2], which provides a direct means of imaging conductive substrates and molecular imaging with sub-nanometer vertical and horizontal resolution. Other *in-situ* topographical methods employed in electrochemical investigations include optical microscopy, scanning electrochemical microscopy[3] and stylus profilometry[4].

Our laboratories have recently explored the use of optical interferometric microscopy to examine electrode topography. *Ex-situ* interferometric techniques have been infrequently used by electrochemists, in part due to the laborious data processing required in numerically computing 3-D images from raw interference intensities. The use of microcomputers removes this obstacle, making image processing possible in tens of seconds to minutes, depending on the size of the area being imaged (vide infra). Optical interferometric microscopes[5,6] that are capable of 3-D surface imaging with vertical resolution of 1 nm or better are commercially available[7,8] and are finding extensive applications in the microelectronics industry, magnetic thin-film processing, and optical machining.

In previous reports, we and others have reported *ex-situ* topographical images of metallic[9] and carbon[10] electrodes obtained using phase-measurement interferometric microscopy, (PMIM). PMIM is a laser interference technique capable of generating 3-D

images from reflecting substrates (> 1% reflectivity). PMIM analyses of electrodes constructed from a single material phase does not require knowledge of the electrode's optical properties.

In the present report, we describe *in-situ* PMIM imaging of electrodes immersed under 0.1 to 0.4 cm of electrolyte solution. We find that the resolution of images of immersed electrodes rivals that in air, allowing high-resolution, *in-situ*, interferometric imaging of electrodes for the first time. The present article focuses on theoretical and experimental considerations required for *in-situ* PMIM; representative examples of PMIM images from on-going electrochemical investigations are presented to demonstrate the performance and utility of this method.

Experimental. *Phase Measurement Interferometric Microscopy.* All measurements were made with ZYGO Maxim·3D Laser Interferometric Microscope (Middlefield, CT), hereafter referred to as a phase-measurement interferometric microscope (PMIM). A detailed description of the microscope and measurement theory is given elsewhere[7]. Briefly, the Maxim·3D system includes the microscope, a processor with input/output devices, a vibration isolation table, and a live video monitor (Fig. 1). Light emitted by a linear polarized 1 mW He-Ne laser (λ = 632.8 nm) is focused onto a rotating diffuser focus lens. The diffuser destroys the spatial coherence to allow exclusion of interference from internal microscope components. The light passes through a back focus lens and reflects off a polarizing beamsplitter. The radiation, now s-polarized, is recollimated by the microscope objective, and proceeds to a second beamsplitter that sends one beam to an optical reference surface and the other to the electrode surface. The difference in distances travelled by these split beams defines the interferometer cavity. Reflected light from the electrode and reference surfaces interfere and is p-polarized by a quarter wave plate above the beamsplitter. The resulting set of spatially resolved intensities are recorded on a 244 x 388 pixel charge injection device (CID) array camera. The digitized output from the CID

camera is analyzed to produce a phase map representing the relative differences in height between the reference and test surfaces. A video monitor connected to the array camera provides a direct optical image of the sample.

Fizeau and Mirau interferometers are used in the measurements reported below (Fig. 2). In the Fizeau interferometer, the beam is split by a partially reflecting film which acts as both beamsplitter and reference surface. The interferometer cavity length, twice the distance from the beam splitter to the test surface, requires a coherence length on the order of millimeters for interference to occur. In the Mirau interferometer (also Fig. 2) the beamsplitter and reference surface are distinct. Because the reference and test arms of the split beam travel approximately the same distance, the Mirau interferometer can be used with light of coherence length on the order of wavelengths.

Certain advantages and disadvantages must be considered in using either the Fizeau or Mirau interferometers to image electrode surfaces. The Mirau interferometer is less susceptible to dust and artifact induced optical aberrations than the Fizeau and is capable of imaging submerged surfaces and distinguishing between different interfaces in thin film materials. The shorter coherence length of the Mirau, however, causes decreased intensity levels and limits the height measurement range. Mirau interferometers generally have lower numerical aperature and therefore greater working distances than Fizeau interferometers, and are limited in magnification by the components attached in front of the objective.

The microscope uses a dynamic phase measurement technique to determine the vertical surface heights. The intensity of light, I, detected by the CID array camera for position (x,y) on the test surface is given by

$$I = I_1 + I_2\cos[\phi(x,y) + \alpha(t)] \qquad (1)$$

I_1 represents the time averaged sum of reflected intensities from the reference and electrode surface. The second term on the right-hand side represents a time varying component of

the interference intensity, where $\phi(x,y)$ is the initial phase difference between reflected wavefronts originating at the electrode and reference surfaces. To measure the vertical heights across the surface, five 90° phase shifts are introduced between the reference and test signals using a piezoelectric transducer to move the reference surface at a constant rate towards the electrode surface[11]. The intensity detected at each pixel of the camera is integrated over each interval during this movement and recorded after phase-changes of $\alpha(t)$ = 90, 180, 270, 360, and 450° between reference and test signals. Integration of the interference intensity over these 5 intervals yields 5 values:

$$A(x,y) = I_1' + I_2'[\cos\phi(x,y) - \sin\phi(x,y)] \quad (2)$$

$$B(x,y) = I_1' - I_2'[\cos\phi(x,y) + \sin\phi(x,y)] \quad (3)$$

$$C(x,y) = I_1' - I_2'[\cos\phi(x,y) - \sin\phi(x,y)] \quad (4)$$

$$D(x,y) = I_1' + I_2'[\cos\phi(x,y) + \sin\phi(x,y)] \quad (5)$$

$$E(x,y) = I_1' + I_2'[\cos\phi(x,y) - \sin\phi(x,y)] \quad (6)$$

from which the spatially dependent phase $\phi(x,y)$ is calculated :

$$\phi(x,y) = \tan^{-1}\left[\frac{(A(x,y) + E(x,y) - 2C(x,y))}{2(B(x,y) - D(x,y))}\right] + \frac{\pi}{4} \quad (7)$$

The variation in optical height across the electrode surface is computed directly from the phase measurement using the equation

$$h(x,y) = (\lambda/4\pi)\phi(x,y) \quad (8)$$

where λ is the wavelength of the illumination. Calculation of $\phi(x,y)$ and construction of the surface image h(x,y) required ~30 s using an MC68000, 32-bit microprocessor.

Electrochemical Cell for In-situ PMIM

A schematic drawing of the electrochemical cell employed for *in-situ* studies is shown in Fig. 3. In order to reduce vibrations, the electrode substrate was mounted on a short glass tube epoxied to the bottom of a 3-inch diameter glass petri dish which served as the cell body. The cell was placed on the motorized x-y stage (controlled by 0.25 μm stepper motors) allowing horizontal translation to observe different regions of the electrode.

The primary source of noise in imaging electrodes under bulk electrolyte is the transient rippling of the air/solution interface resulting from natural convection and mechanical vibration. A non-planar air/solution interface introduces spatially-dependent differences in the optical distance between the interferometer reference and the electrode surface that cannot be distinguished from variations in optical distances produced by the surface topography. The signal noise resulting from fluid convection is sufficiently large to prevent image analysis of 10 nm vertical structures. However, filling the cell with 3 mm spherical glass beads (Fig. 3) effectively eliminates this problem. Further reduction in noise is gained when a glass cover plate, with a hole provided for the microscope objective, is placed on top of the cell. This procedure reduces the effects of stray air currents and acoustic vibrations.

Electrodes and Chemicals. Platinum thin film electrodes were prepared by rf sputter deposition of Pt onto freshly cleaved muscovite mica. Details of film deposition have been presented elsewhere[12]. Specimens of highly oriented pyrolytic graphite were obtained from Union Carbide. Iron disk electrodes were prepared by sealing a 1mm diameter Fe wire (Alpha) in a glass tube. These electrodes were polished successively with 5, 1 and 0.05 μm alumina and chemically etched using 3% nitric acid in methanol to expose grain boundaries.

Aqueous solutions were prepared from 18MΩ H_2O purified using a Conoco Water Prodigy System.

Results and Discussion.

PMIM images are based on measurements of differences in the optical path length between the test substrate and the optical reference surface located at the base of the microscope objective. In order to measure the topography of the substrate constructed from a single homogeneous phase, it is necessary to know the refractive index of the medium in contact with the substrate. To illustrate this, we show in Fig. 4 the situation encountered for *in-situ* imaging of electrodes submerged under a bulk layer of electrolyte. The optical paths are traced between the substrate and reference surface at two locations on the surface (x,y and x',y') that differ in physical height by the distance z. An assumption in the analysis is that the average plane of the reference surface is parallel to the plane defining the air/electrolyte interface.

The optical path length, d_T, between the substrate and reference surface at x,y and x',y' is given by:

$$d_T(x,y) = d_{air}n_{air} + d_{H_2O}n_{H_2O} \quad (9)$$

$$d_T(x',y') = d_{air}n_{air} + d_{H_2O}n_{H_2O} - zn_{H_2O} \quad (10)$$

where n_{air} and n_{H_2O} are the refractive indices of air and H_2O (or an electrolyte solution), and d_{air} is the distance between the air/electrolyte interface and reference surface. Subtraction of eq. (10) from (9) yields

$$z = (d_T(x,y) - d_T(x',y'))/n_{H_2O} = h(x,y)/n_{H_2O} \quad (11).$$

Measurement of d_T for all x,y positions and correcting these values for the refractive index of the covering medium yields a topographical image of the substrate. It is important to note that neither the optical properties of the substrate or the thickness of the electrolyte layer are required in the analysis which greatly simplifies the measurement. In our studies, we generally use a electrolyte layer of thickness between 2 and 4 mm which allows a working distance of ~2-4 mm between the microscope objective and the solution.

Figure 5 shows PMIM images of the basal plane of freshly cleaved highly ordered pyrolytic graphite (HOPG) . The large area (4125 μm^2) image in Fig. 5(a) was taken in air with a 40x Mirau objective and shows several well-defined steps, ranging in vertical height from ~10 to 100 nm, that expose the edge plane of HOPG. Measurement of the horizontal length and the vertical height of each observable step yields an exposed area of edge plane HOPG of ~ 20μm^2, which represents 0.5 % of the projected geometric electrode surface. The images shown in Fig. 5 (b) and (c) are also of the basal plane of a HOPG but were obtained with the substrate submerged under 3 mm H_2O using the cell shown in Fig. 3. The edge plane area obtained from these images represents between 0.3 and 0.7 % of the projected area.

PMIM imaging is not limited to electrically conductive or highly reflective metal substrates. The only requirement for analysis is that the sample be partially reflecting. For example, Fig. 6 shows images of a polished glass lens taken at different magnifications using 10X and 40X Mirau and 100X Fizeau objectives. The 20 to 100 nm deep groves, oriented from the top to bottom of the image, result from surface polishing.

Fig. 7 shows an image, in 0.1 M KCl, of a 10 nm thick Pt film which has been sputtered deposited on cleaved muscovite mica. There are no discernable differences between the PMIM images in air and 0.1 M KCl. Although Pt deposits on mica as a uniformly thick polycrystalline film, step sites such as the one in Fig. 7 are occasionally observed which result from surface steps on the underlying substrate. Mica has a natural cleavage plane parallel to the Van der Waals surface and can be cleaved to produce a nearly

atomically smooth surface with few edge steps. This surface feature has been used to quantitatively compare vertical height measurements in air with those in a 0.1 M KCl solution. The lower half of Fig. 7 shows profiles of the step for both media (taken from right to left near the middle of the image) after accounting for the differences in the refractive indices of air and water. These surface profiles are nearly identical (within 0.5 nm) indicating that the aqueous layer has an insignificant effect on the optical quality of the images. The image in Fig. 7 was repeatedly obtained over a period of several hours and with different thicknesses of electrolyte covering the surface without any noticeable change.

Fig.8 shows a comparison of PMIM images of a polycrystalline Fe surface taken in air and submerged under ~2 mm of H_2O. The rectangular protrusion above the surface represents an individual grain of Fe surrounded by a surface region that has been preferentially etched in 3% HNO_3/methanol. Similar to the above profiles of Pt, the images in Fig. 8 show that there are essentially no differences in the quality of PMIM images obtain in air or H_2O.

In a previous report[3], we demonstrated that PMIM could be used to examine corrosion pits on Fe resulting from brief exposures to 0.1 M H_2SC_4. The measurements were made *ex-situ*, following a 5 sec. immersion of a 100 μm diameter Fe disk to the acid solution, rinsing with distilled H_2O, and air drying. Fig. 9 shows a similar set of measurements made on a macroscopic Fe sample (1mm diameter) that was previously etched in 3% HNO_3/methanol, and that is fully immersed underneath ~2mm of 0.1 M H_2SO_4. Fig. 9a is a large area PMIM image of the Fe surface recorded within 10 sec. of sample immersion. Fig. 9b shows a smaller region of the same surface located toward the left corner of Fig. 9a. The boundaries between three Fe grains are clearly evident, with the grain surface in the foreground located ~150nm below the two other grains. The topography of the central flat grain region in the foreground is shown as a function of immersion time is shown in the sequence of images plotted in Fig. 9c. In these images, the z-direction is inverted in order to allow better viewing of pits that develop in the sample.

The image labeled "initial" represents the measurement immediately following sample immersion and is taken from the same data set as plotted in Figs. 8a and b. This image shows that the grain surface is initially very smooth with broad features with vertical heights on the order of 10 nm. Beginning with the image taken at 9 min., the sequence shows the development of surface depressions (which appear as hills in the inverted images) of base diameter between 3-5 μm. These depressions, which result from the local dissolution of Fe, are qualitatively similar in shape and in size to the pits observed in the *ex-situ* images described above. However, there are 2 notable differences between the images obtained in the *ex-situ* and *in-situ* measurements. In the former, pits with depths on the order of 40 nm were recorded after only a total of 20 sec. total immersion in 0.1 M H_2SO_4. In contrast, the images in Fig. 9c show that the rate of pit growth is considerably slower (with pitting occurring after ~10-15 min) when the sample remains fully immersed in the solution. The second difference that is apparent in the *in-situ* images is the presence of hills adjacent to the pits which develop at a rate qualitatively similar to that of the pits. We speculate that these regions may represent the build-up of corrosion products surrounding the pit which, in the previous studies, were rinsed away in preparation of the sample for *ex-situ* analyses. Regardless of the origin of these features, the images presented in Fig. 9c demonstrate a significant difference in the corrosion rate of Fe samples continuously immersed and those intermittently immersed and rinsed.

Conclusion. Topographical imaging of a variety of electrode materials using PMIM has been demonstrated. The advantages of PMIM relative to other existing topographical methods include: rapid and non-destructive image acquisition, the ability to image non-conducting materials, and the ability to image surfaces submerged in bulk electrolytes. This latter feature allows potential and time-dependent features on electrodes to be monitored *in-situ*. The single optical parameter required in image analysis is the refractive index of the fluid in which the sample is immersed; neither the height of the fluid above the

test substrate nor the optical properties of the substrate enter the analysis of electrodes constructed from single material. Quantitative comparison of PMIM images taken in air and in aqueous electrolytes demonstrates that the electrolyte does not significantly degrade image quality provided fluid convection is absent or minimized. In the following article in this volume, we consider PMIM imaging of multicomponent subtrates and metallic substrates coated by an oxide film of thickness less than the coherence length of the light used in the PMIM system. Analyses of these systems require optical parameters of the test sample.

Figures.

1. Schematic diagram of PMIM optical system.

2. Schematic comparison of 40X Mirau and 100X Fizeau interferometers.

3. Schematic drawing (approximately to scale) of the electrochemical cell used for *in-situ* PMIM imaging. The circles represent 3 mm glass beads placed in the electrolyte to reduce fluid convection. The microscope and cell are supported by a vibration isolation table.

4. Optical distance in interferometric imaging of electrodes submerged under fluid electrolytes.

5. PMIM images of highly ordered pyrolytic graphite: (a) in air; (b) and (c) in H_2O . Images taken with 40X Mirau objective.

6. PMIM images in air of a polished glass optical lens using (A) 10X Mirau; (B) 40X Mirau; and (C) 100 X Fizeau objectives.

7. Image of a step on a thin film Pt electrode immersed in 0.1 M KCl. The bottom plot shows the vertical profiles across the step obtained in air (•) and in 0.1 M KCl (o). 40X Mirau objective.

8. Images of an etched Fe electrode in air and H_2O . The raised area is a single Fe grain protruding above the surrounding grains. 40X Mirau objective.

9. PMIM images of an etched Fe electrode immersed in 0.1 M H_2SO_4 as a function of time. Fig. (A) shows a large area image immediately following immersion of the electrode.

Fig. (B) is an enlargement of the top left corner of Fig. A. The sequence of images shown in Fig. (C) corresponds to the central lower region of Fig. (B) following immersion. The images in Fig. (C) have been inverted (i.e., hills represent valleys) to clearly show the growth of pits as a function of time. All images were obtained using a 40X Mirau objective.

CREDIT. Financial support for this work was provided by an Instrumentation grant from the National Science Foundation, CBT-8807676, and by the Department of Energy-Office of Basic Energy Science, DE-FG02-88ER45338. H.S.W. gratefully acknowledges support from the Office of Naval Research Young Investigator Program.

References.

1. Binning, G., Rohrer, H., *Helv. Phys. Acta* **1982**, *55*, 726.

2. Binning, G., Rohrer, H., Gerber, Ch. Weibel, E., *Appl. Phys. Lett.* **1982**, *40*, 178.

3. Kwak, J. and Bard, A. J., *Anal. Chem.*, **1989**, *61*, 1794.

4. Lewis, T. J., White, H. S., Wrighton, M. S., *J. Am. Chem. Soc.*, **1984**, *106*, 6947.

5. Perry, D. M., Morgan, P. J.; Robinson, G. M., *J. Inst. Electr. Rad.* **1985**, *55*, 45.

6. Perry, D. M, Robinson, G. M.; Peterson, R. W., *IEEE Trans. Magnet*, **1983**, *19*, 1656.

7. Biegen, J. F. and Smythe, R. A., *SPIE O/E LASE '88 Sym. on Optoelect. and Laser Appl. in Sci. and Eng.*, Jan. 1988, Los Angeles, CA.

8. Wyant, J. C., Creath, K., Prettyjohns, K. N., *Proceedings of the 2nd International Machine Tool Engineering Conference*, Nov. 4, 1985, Osaka, Japan.

9. Kragt, H. J.; Earl, D. J.; Norton, J. D.; and White, H. S., *J. Electrochem. Soc.*, **1989**, *136*, 1752.

10. Smyrl, W. H., Atanasoski, R. T., Atanasoska, Lj., Hartshorn, L., Lien, M., Nygren, K., and Fletcher, E. A., *J. ELectroanal. Chem.* **1989**, *264*, 301.

11. Hariharan, P., Oreb, B. F., and Eiju, T., *Appl. Opt.* **1987**, *26*, 2504.

12. Smith, C. P., Maeda, M., Atanasoska, Lj., White, H. S., and McClure, D. J., *J. Phys. Chem.* **1988**, *92*, 199.

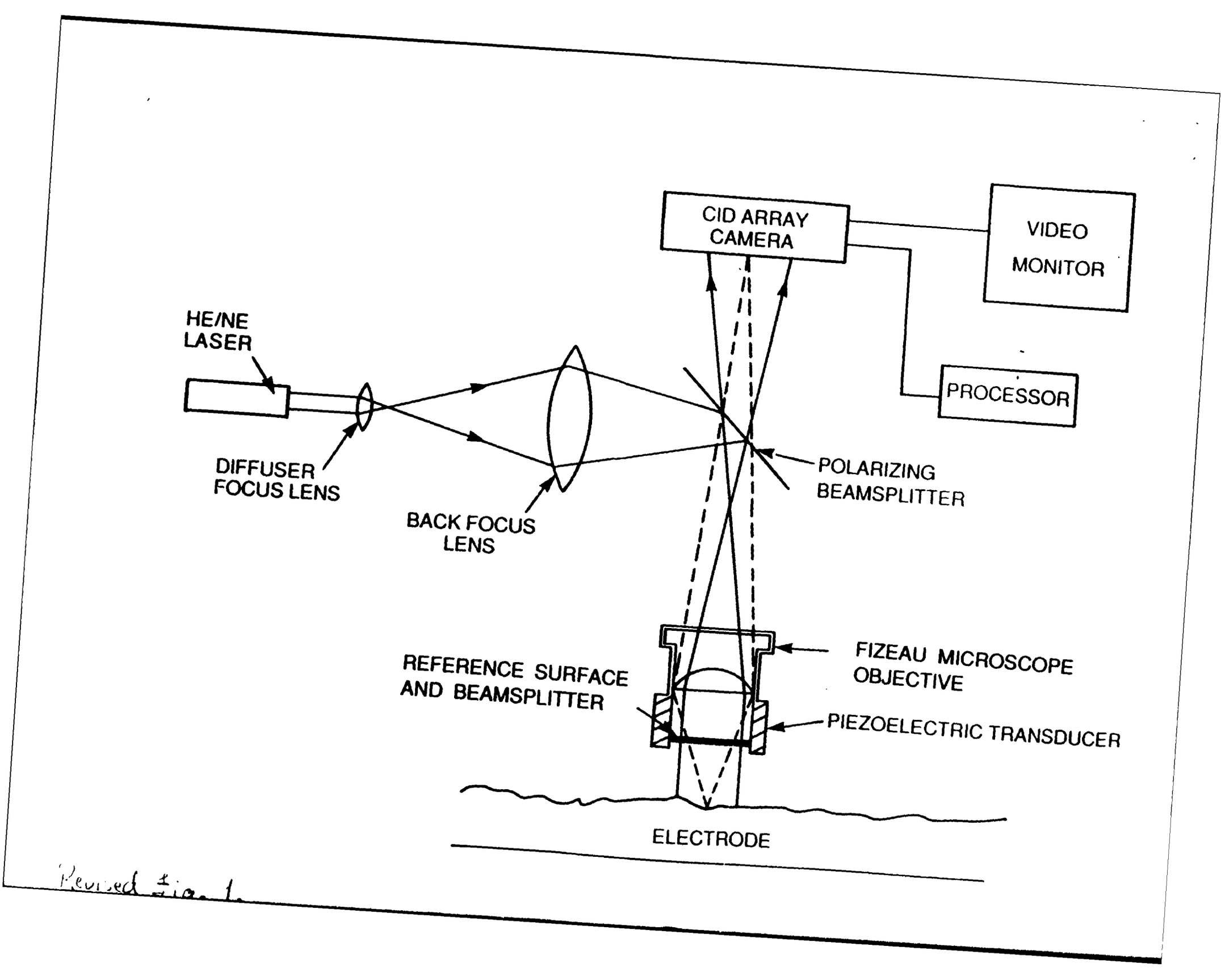

Revised Fig. 1.

FIZEAU

Unequal Path Length Interferometer

Coherence length ≈ 1mm

MIRAU

Equal Path Length Interferometer

Coherence length ≈ 1μm

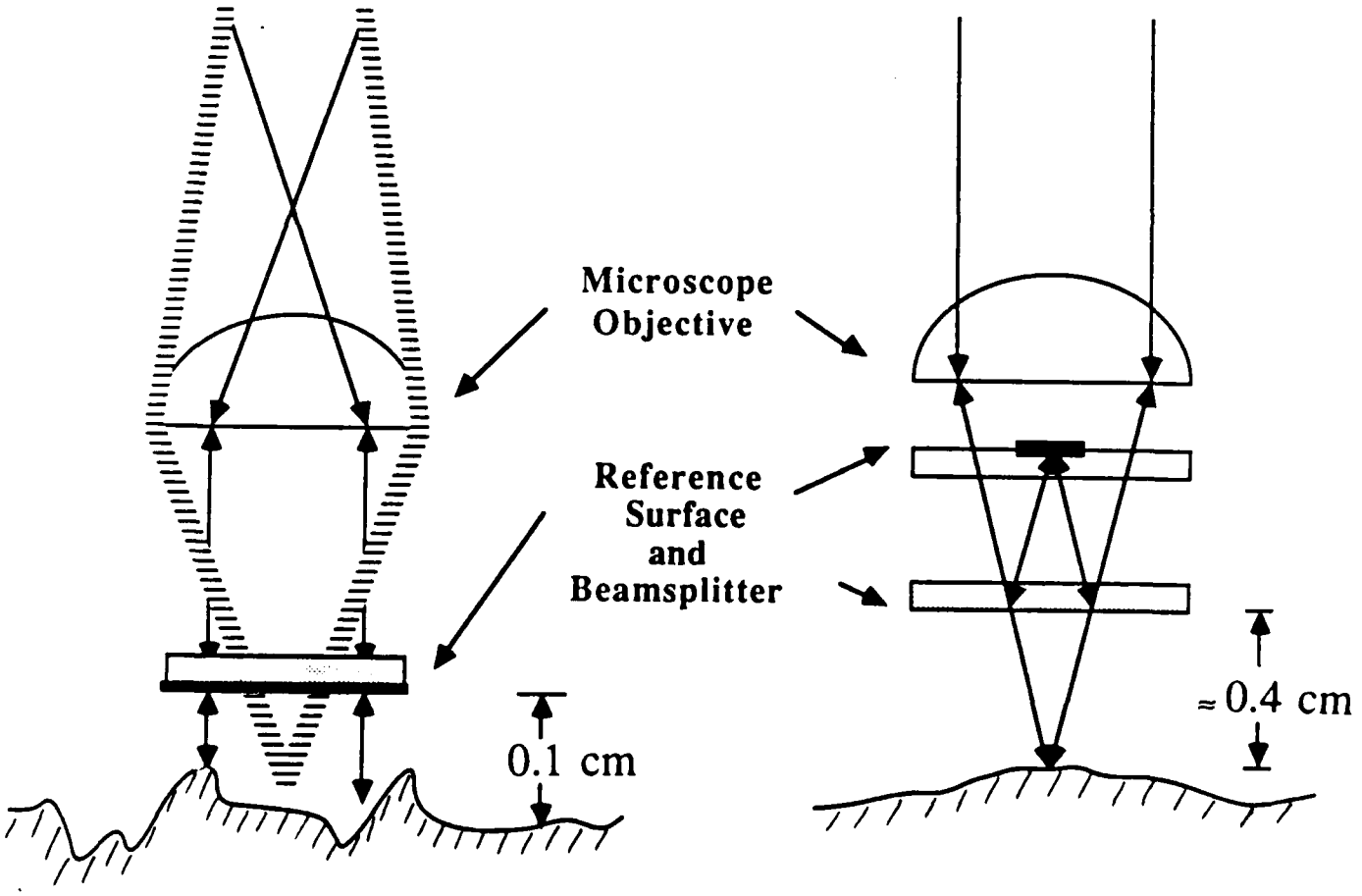

Fig 2

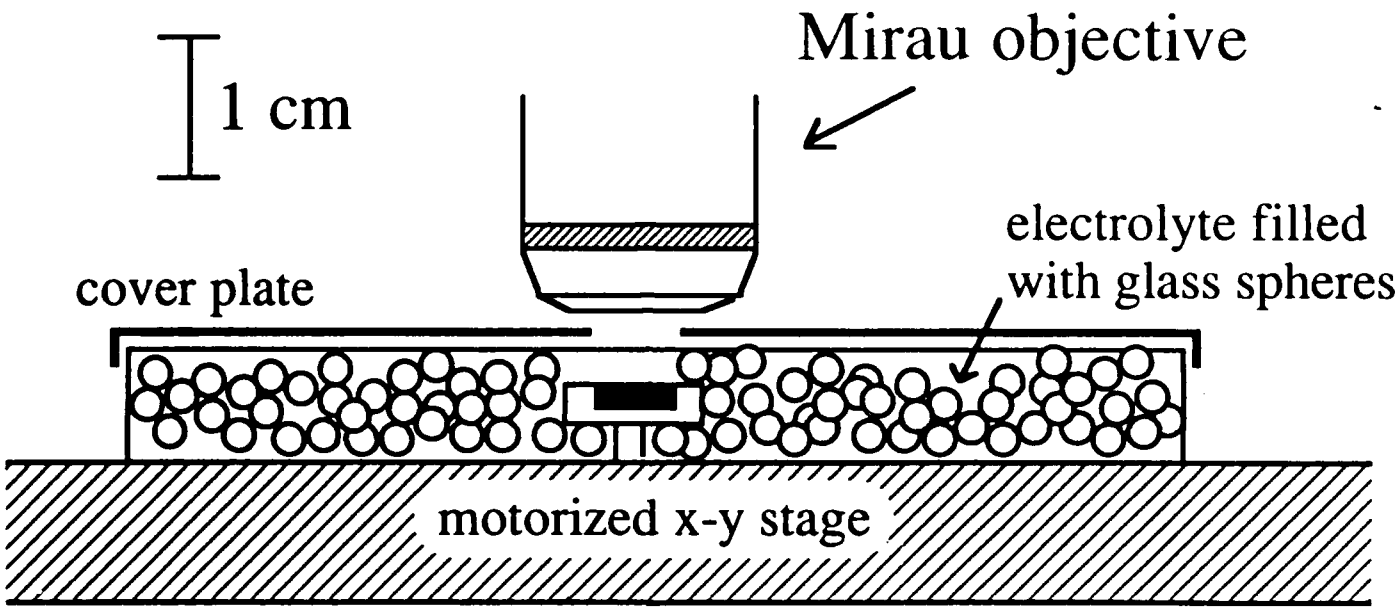
1 cm
Mirau objective
electrolyte filled
with glass spheres
cover plate
motorized x-y stage

Fig 3

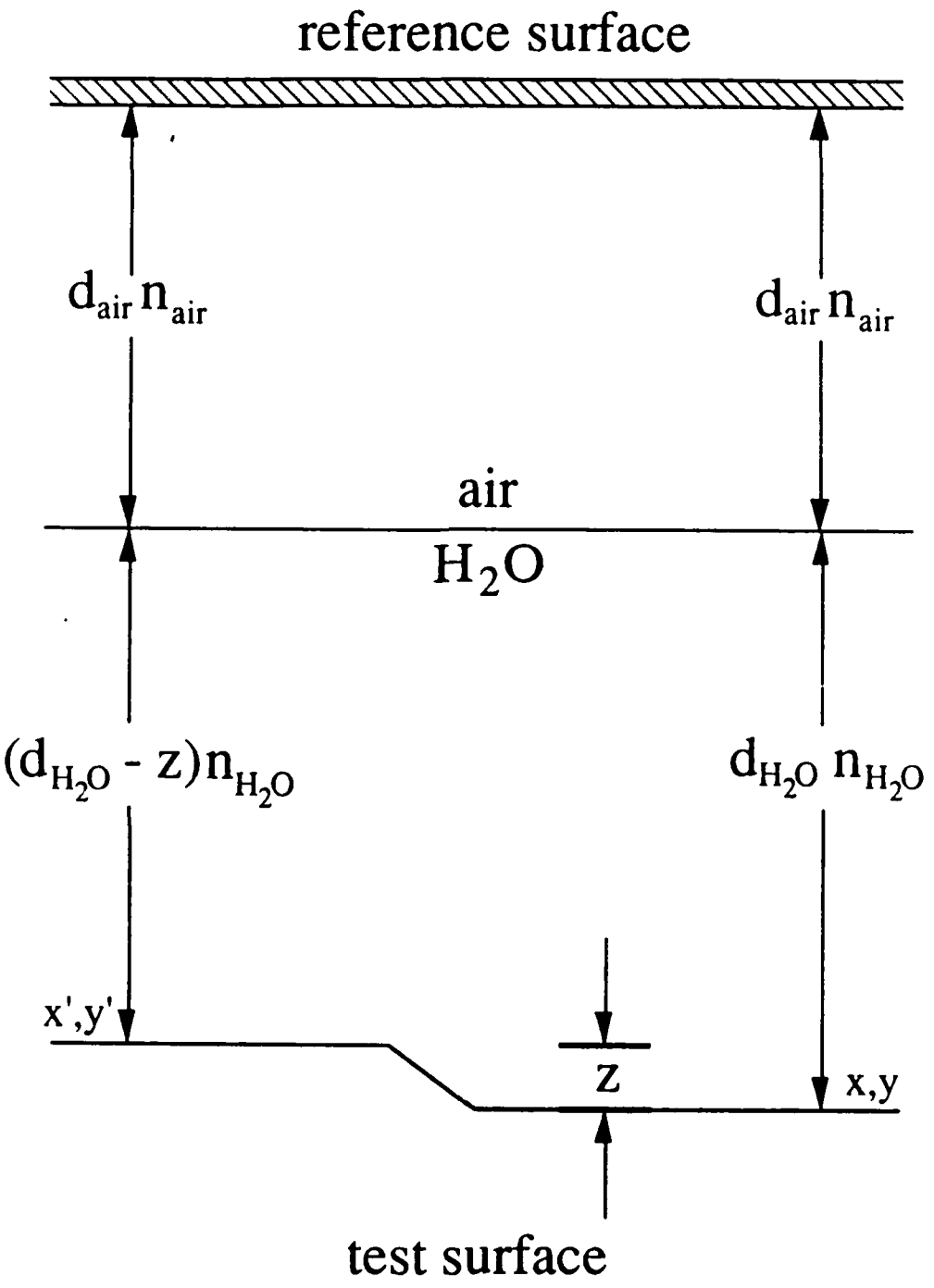
reference surface
$d_{air}\, n_{air}$
$d_{air}\, n_{air}$
air
H_2O
$(d_{H_2O} - z)n_{H_2O}$
$d_{H_2O}\, n_{H_2O}$
x',y'
z
x,y
test surface

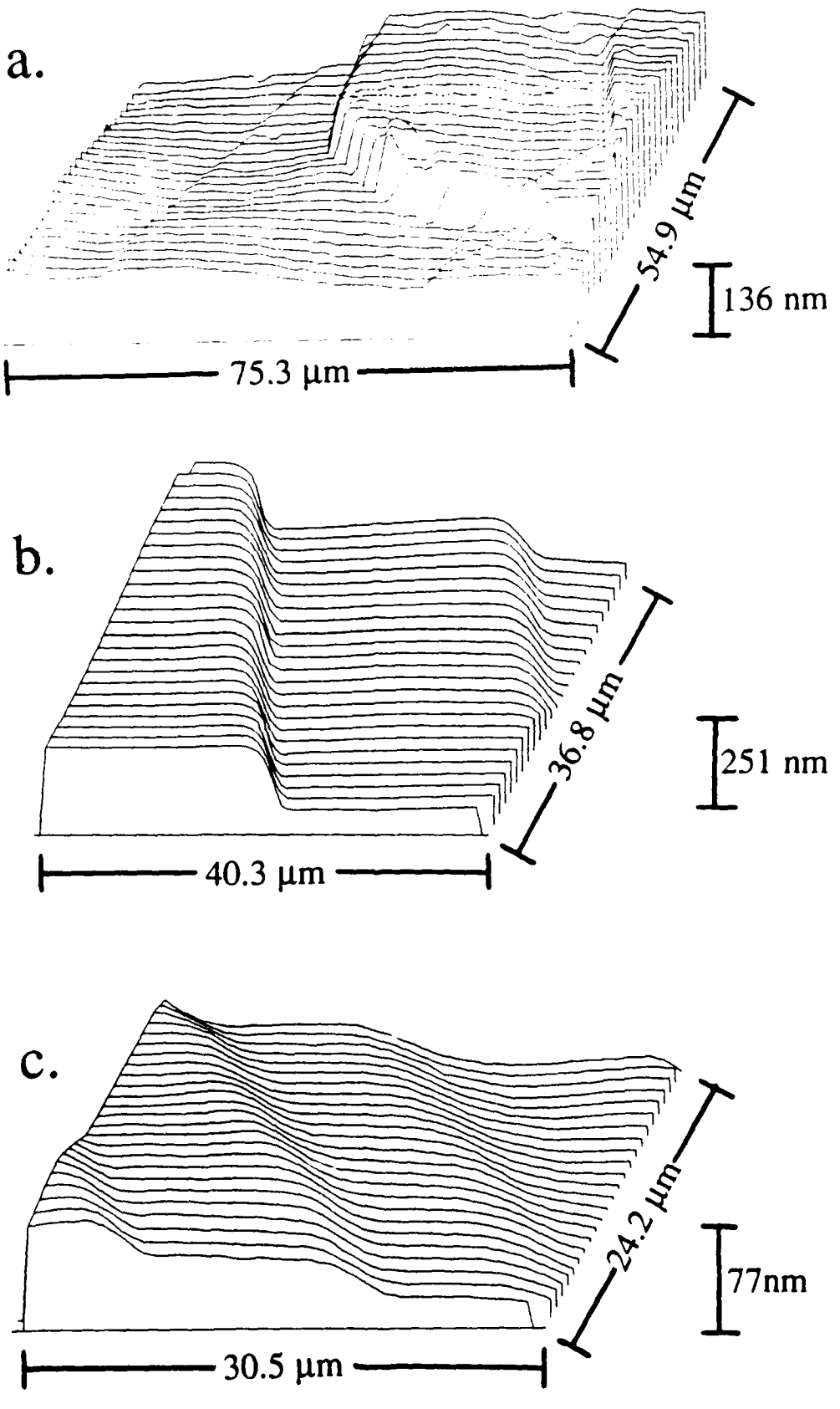

Fig 5

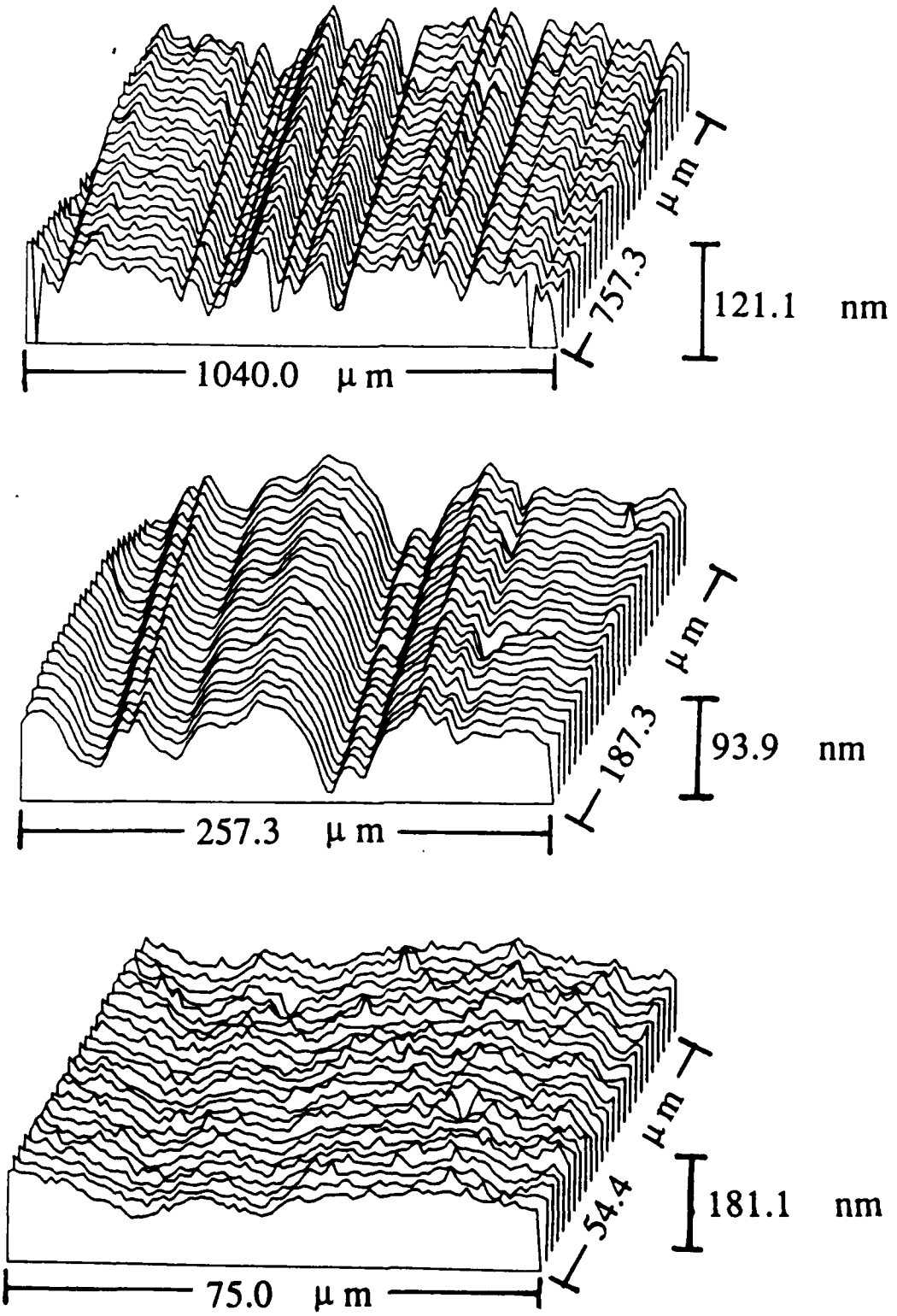
1040.0 μm
757.3 μm
121.1 nm
257.3 μm
187.3 μm
93.9 nm
75.0 μm
54.4 μm
181.1 nm

Fig 6

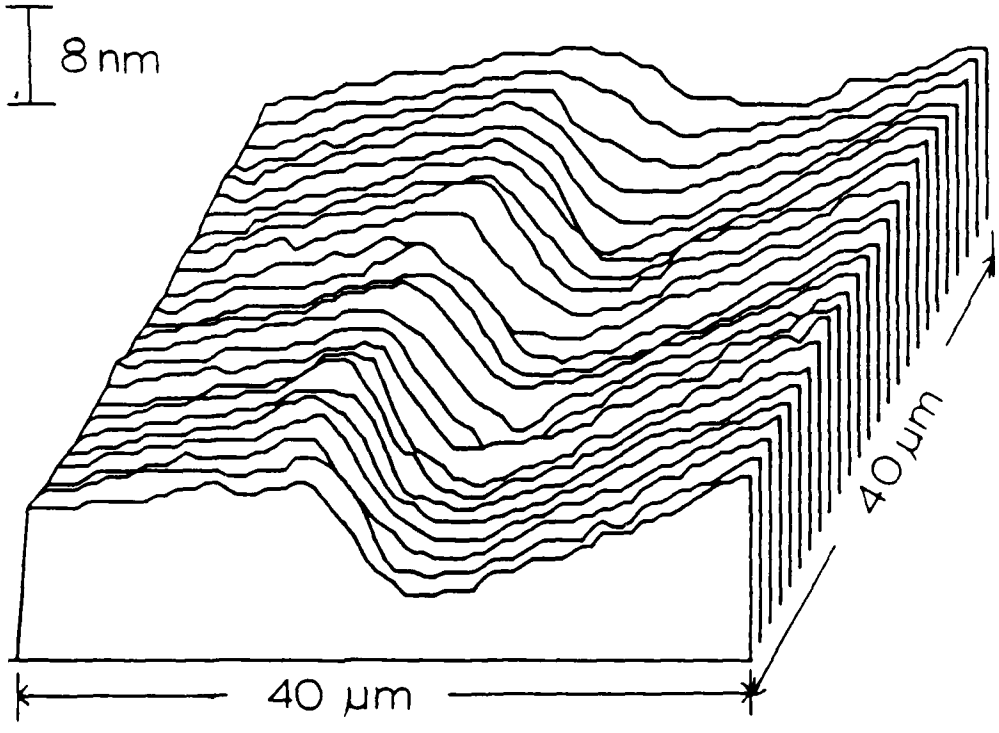

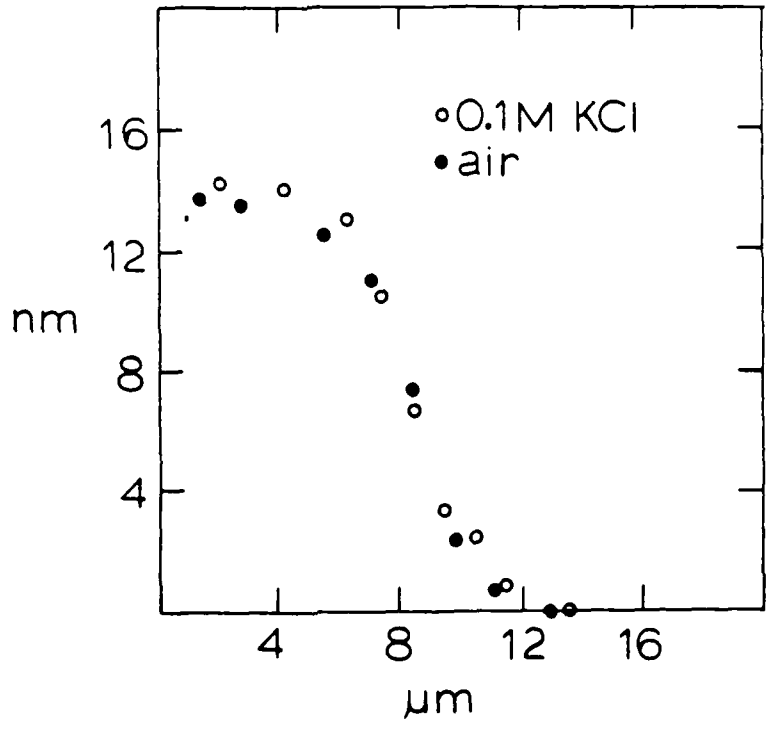

Fig 7

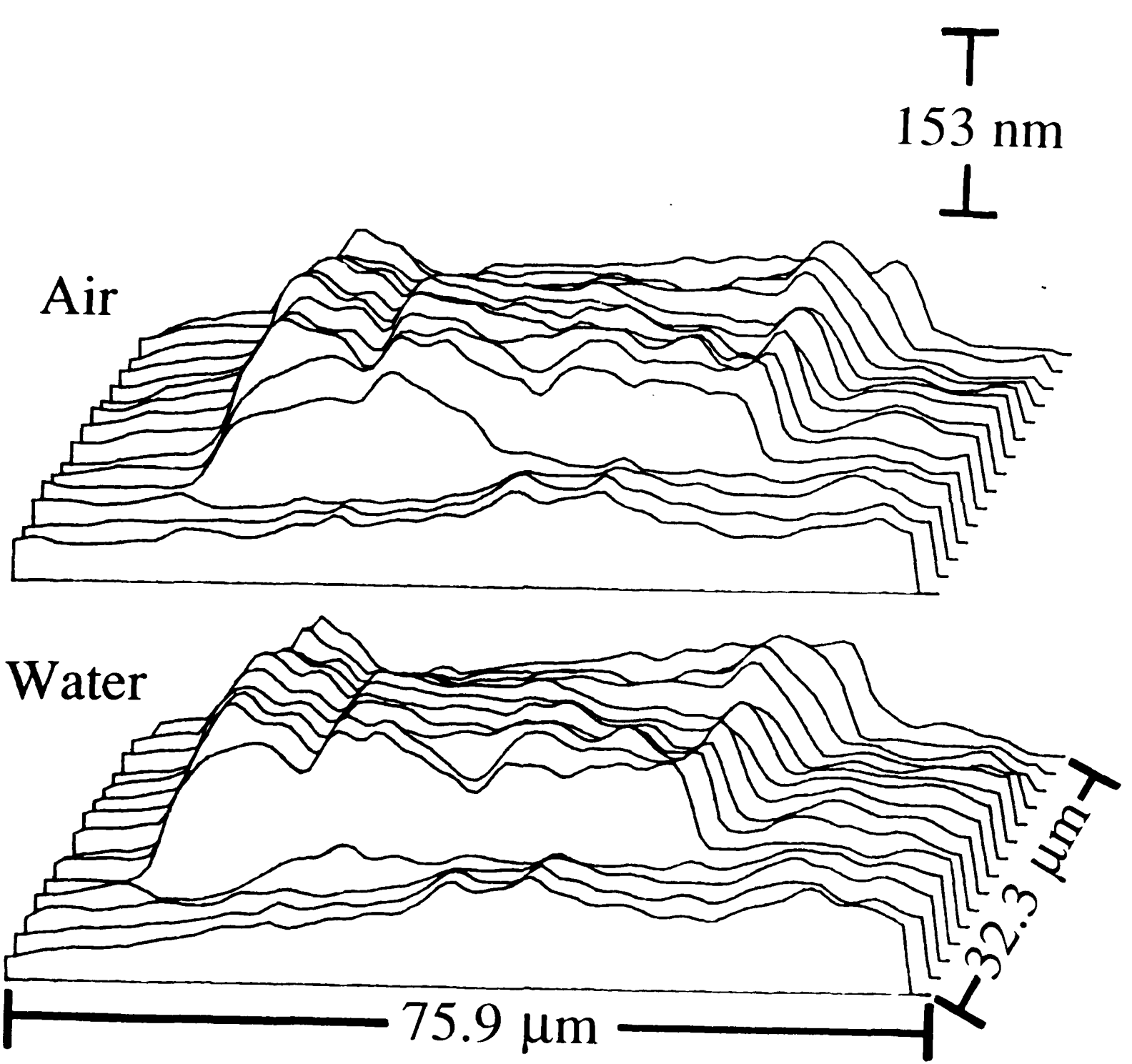

Fig. 8

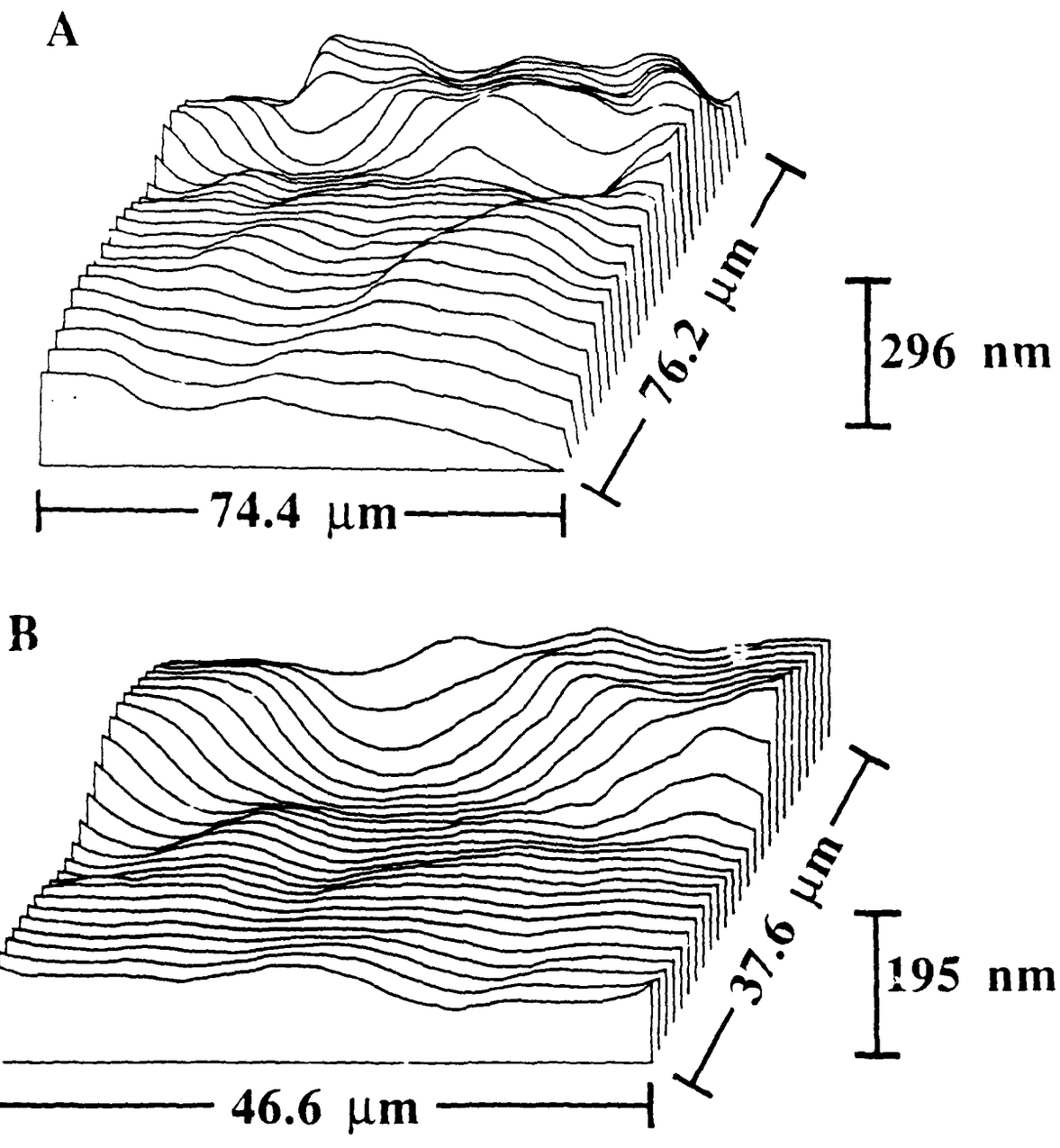

Fig 9A & B

C

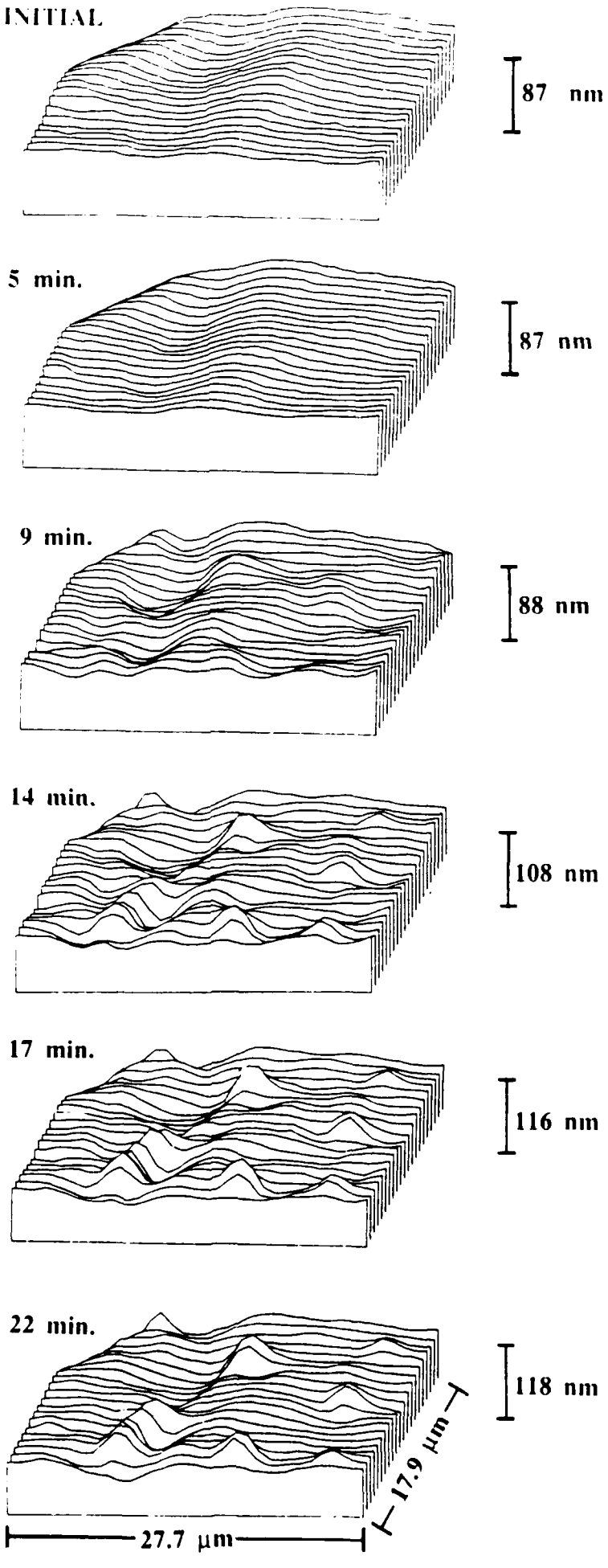
INITIAL
87 nm
5 min.
87 nm
9 min.
88 nm
14 min.
108 nm
17 min.
116 nm
22 min.
118 nm
17.9 µm
27.7 µm

Fig 9C